Micro-electrode to metal surface distance determination
by Uri James Rogers

A thesis submitted in partial fulfillment of the requirements for the degree of Master of Science in Electrical Engineering
Montana State University

Abstract:
The analysis of microbial ecology and surface chemistry at a microscale level requires that ion-sensitive microelectrodes, such as pH, Sulfide, and Dissolved Oxygen, be non-destructively positioned within one to five micrometers of a metal surface/coupon. Because microelectrodes measure profiles through a biofilm the distance between the electrode tip and the metal coupon must be known at all times. This is needed so that the biofilm structure can be accurately analyzed and to ensure that the electrode and metal surface do not destructively come into contact with one another.

Three methods were developed to solve this problem: 1) the electrode capacitance 2) the disk capacitance 3) the short circuit resistance. The first two procedures use theoretical models to relate capacitance to distance, while the third method uses the short circuit phenomenon that occurs between two metal objects that come into contact.

Both the capacitance techniques produced electrode distance to surface measurements that had deviations of 50 to 150 micrometers from the approximated distance. These deviations were caused by electrical parasitic effects as well as fluctuations in the thickness of the electric double layer with temperature. The short circuit resistance method, however, does not suffer from these effects and allows the distance to be measured to within five micrometers.

Of the three methods, the short circuit resistance method has the highest accuracy and is the easiest to use. This is because it does not suffer from the parasitic effects and temperature fluctuations apparent in the capacitance techniques.

MICRO-ELECTRODE TO METAL SURFACE DISTANCE DETERMINATION

by

Uri James Rogers

A thesis submitted in partial fulfillment
of the requirements for the degree

of

Master of Science

in

Electrical Engineering

MONTANA STATE UNIVERSITY
Bozeman, Montana

April 1992

APPROVAL

of a thesis submitted by

Uri James Rogers

This thesis has been read by each member of the thesis committee and has been found to be satisfactory regarding content, English usage, format, citations, bibliographic style, and consistency, and is ready for submission to the College of Graduate Studies.

4-22-92
Date

Chairperson,Graduate Committee

Approved for the Major Department

4-22-92
Date

Head, Major Department

Approved for the College of Graduate Studies

4/28/92
Date

Graduate Dean

STATEMENT OF PERMISSION TO USE

In presenting this thesis in partial fulfillment of the requirements for a master's degree at Montana State University, I agree that the Library shall make it available to borrowers under rules of the Library. Brief quotations from this thesis are allowable without special permission, provided that accurate acknowledgment of source is made.

Permission for extensive quotation from or reproduction of this thesis may be granted by my major professor, or in his absence, by the Dean of Libraries when, in the opinion of either, the proposed use of the material is for scholarly purposes. Any copying or use of the material in this thesis for financial gain shall not be allowed without my written permission.

Signature 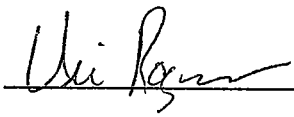

Date 4-22-92

TABLE OF CONTENTS

TABLE OF CONTENTS-Continued

LIST OF TABLES

LIST OF FIGURES

LIST OF FIGURES -- Continued

ABSTRACT

The analysis of microbial ecology and surface chemistry at a microscale level requires that ion-sensitive microelectrodes, such as pH, Sulfide, and Dissolved Oxygen, be non-destructively positioned within one to five micrometers of a metal surface/coupon. Because microelectrodes measure profiles through a biofilm the distance between the electrode tip and the metal coupon must be known at all times. This is needed so that the biofilm structure can be accurately analyzed and to ensure that the electrode and metal surface do not destructively come into contact with one another.

Three methods were developed to solve this problem: 1) the electrode capacitance 2) the disk capacitance 3) the short circuit resistance. The first two procedures use theoretical models to relate capacitance to distance, while the third method uses the short circuit phenomenon that occurs between two metal objects that come into contact.

Both the capacitance techniques produced electrode distance to surface measurements that had deviations of 50 to 150 micrometers from the approximated distance. These deviations were caused by electrical parasitic effects as well as fluctuations in the thickness of the electric double layer with temperature. The short circuit resistance method, however, does not suffer from these effects and allows the distance to be measured to within five micrometers.

Of the three methods, the short circuit resistance method has the highest accuracy and is the easiest to use. This is because it does not suffer from the parasitic effects and temperature fluctuations apparent in the capacitance techniques.

Chapter 1

INTRODUCTION

The analysis of microbial ecology and surface chemistry at a microscale level requires that ion-sensitive microelectrodes be non-destructively positioned within 1 to 5 micrometers (μm) in all three dimensions (X,Y,Z) above a metal coupon. These electrode types include pH, Sulfide, Chloride and Dissolved Oxygen (DO).[1,2] Because microelectrodes measure chemical profiles perpendicularly to the metal surface the distance between the electrode tip and the metal-water interface must be known at each measurement site. An example of this is the dissolved oxygen profile shown in Figure 1. This figure clearly shows the aerobic (high oxygen concentration) conditions at distances greater than 400 μm above the surface and the anaerobic (oxygen depleted) conditions at the metal surface. To accurately model such distributions, the distance to the surface must be known at every measurement site. Positioning an electrode in the two dimensions that are parallel to the metal coupon is trivial and can be accomplished with a large number of X-Y positioning tables. The determination of the perpendicular distance, however, is very complex in nature, particularly within a natural environment such as a biofilm reactor. These complexities stem from the fact that the electrode tip diameter is usually very small ($<30\ \mu$m), submerged in a water based solution, and concealed by biofilm growth

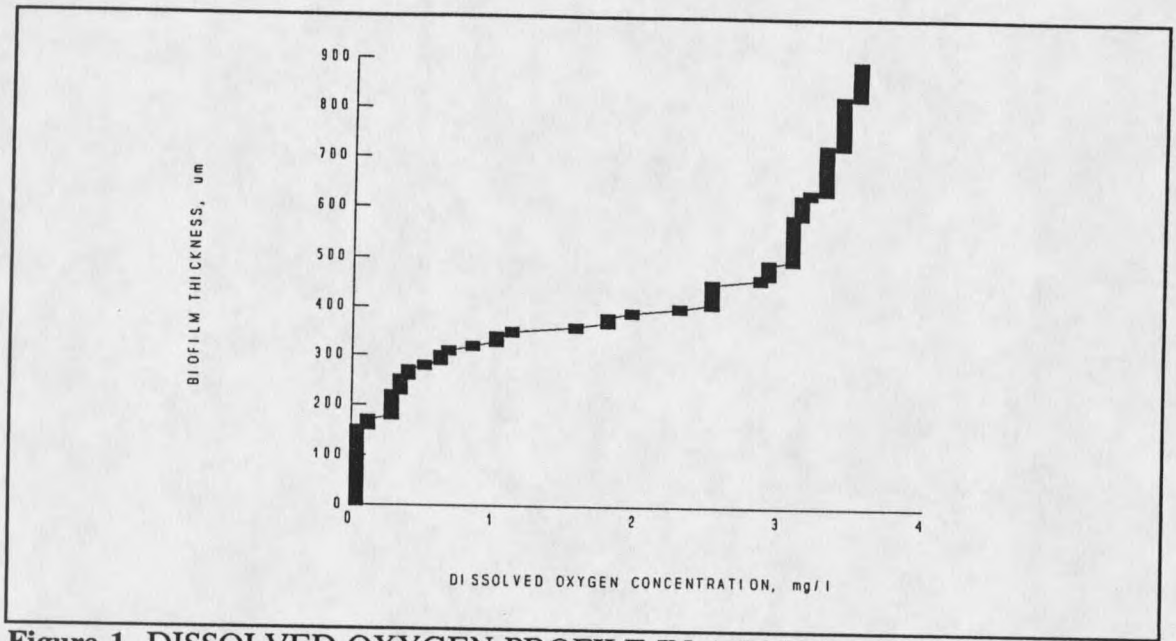

Figure 1 DISSOLVED OXYGEN PROFILE IN A BIOFILM -- as measured by a Dissolved Oxygen Microelectrode, courtesy of the Center for Interfacial Microbial Processes Engineering

and/or corrosion near the interface.

This thesis discusses three methods to measure the distance between an electrode and a metal-water interface: 1) the electrode capacitance 2) the disk capacitance 3) the short circuit resistance. The first two procedures for distance determination use capacitance measurements, which relate theoretical capacitance models to the measured capacitance and the distance to the interface. The third method is based on the short circuit resistance that occurs between two metal objects when they contact one another. The accuracies, limitations, and tradeoffs between the three methods are discussed as well as possible applications and future work.

Chapter 2

ELECTRODE CAPACITANCE

The microelectrodes which are constructed to perform surface chemistry experiments consist of a thin metal wire encased in a glass capillary with the excess glass at the tip ground away to expose the metal wire (Figure 2).[1]

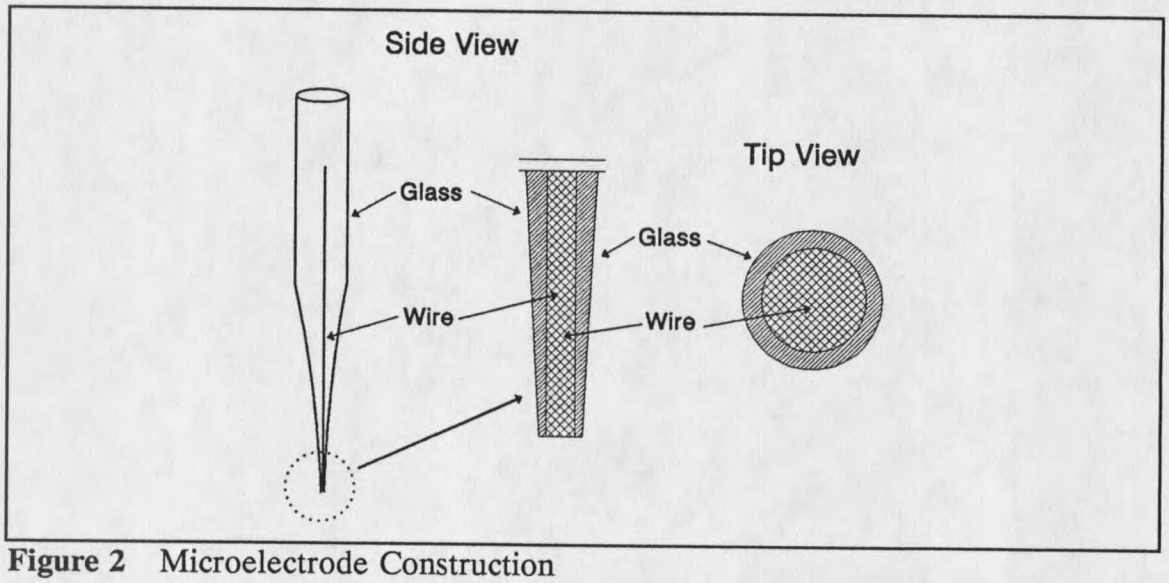

Figure 2 Microelectrode Construction

The basic microelectrode construction lent itself to two general theories to explain the relationship between distance and capacitance. The first theory approximated the capacitance as a quasi-point charge at a height *h* above an infinite conducting plane. A quasi-point is defined as a distinct volume of radius *r* with a

uniform charge distribution throughout.[3] It can be shown that if $r < 5h$ the quasi-point charge can be replaced by an ideal point charge.[3] The calculation of capacitance between a point charge and the conducting plane is determined using the method of images and replacing the plane with a second point charge of opposite polarity at a distance $-2h$ from the first point charge.[4] The capacitance model as well as the image transformation is shown in Figure 3.

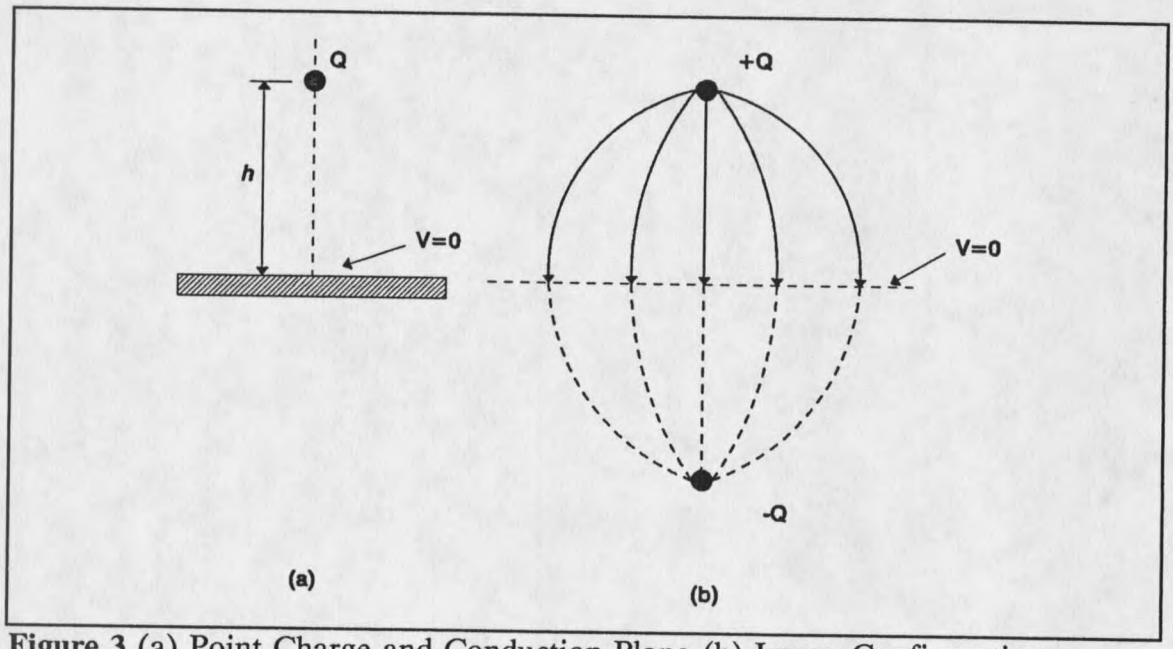

Figure 3 (a) Point Charge and Conduction Plane (b) Image Configuration

Calculating the electric field and potential function shown in 2b provides a relationship between distance and capacitance by:[3]

$$C = 8\pi \epsilon_o \epsilon_r h \qquad (1)$$

where C is the capacitance, ϵ_o is the permittivity of free space, ϵ_r is the relative dielectric constant, and h is the height of the charge above the metal plane. Equation 1 shows that the capacitance in the point charge model is directly related to the distance between the point and the surface.

Electrode Experimental

The hypothesis for the quasi-point charge was analyzed by using an experiment which measured the actual capacitance between the electrode tip and the metal surface. A standard platinum electrode with tip diameter of $\approx$ 30 micrometers (μm) was placed over a stainless steel coupon with a 1.6 centimeter (cm) diameter. The coupon was held in a rectangular reactor containing approximately three cm. of tap water at room temperature. The electrode and the coupon were then connected to a Hewlett Packard (HP) 4800A Vector Impedance Meter so that the capacitance could be measured as the electrode was positioned at various distances relative to the coupon using a Micro Kinetics (see Appendix A) computer controlled XYZ positioning system. The setup, including the electrode, reactor, positioner, and impedance meter, is displayed in Figure 4.

The capacitance of the system was recorded by lowering the probe towards the coupon in 10 μm increments while measuring the capacitance at each interval. The distance between the electrode and the metal surface was determined at each interval in the following manner. The computer positioning system allowed the starting point and step size interval to be recorded while the final point was

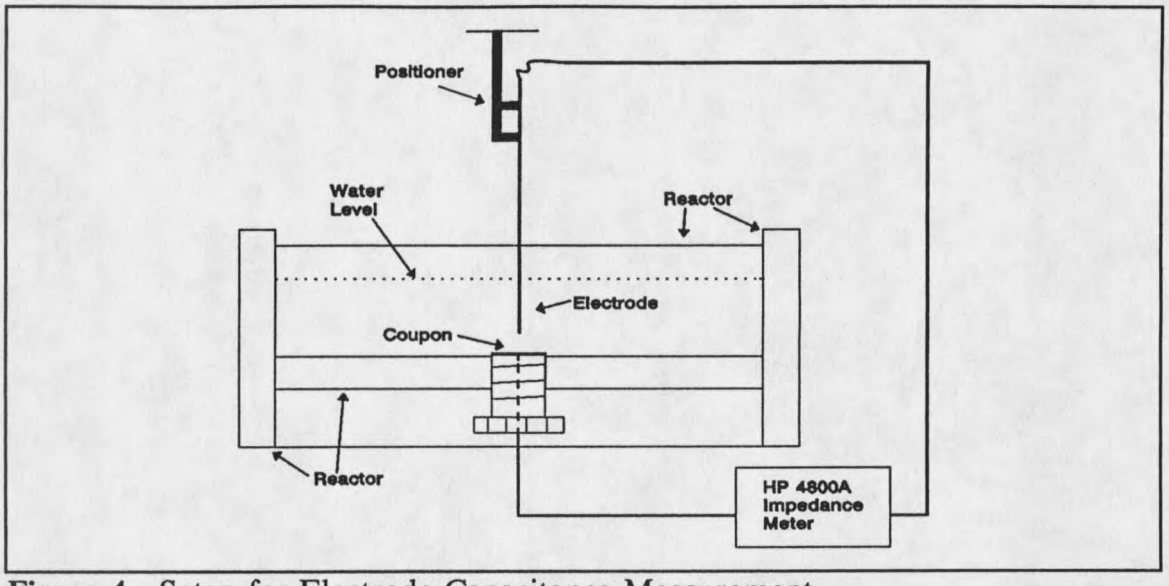

Figure 4 Setup for Electrode Capacitance Measurement

determined by actually touching the probe to the surface. At the point of contact, the impedance measured decreased sharply, almost to zero, which allowed the position to be approximated with a +/- 5 μm degree of accuracy. Knowing the two endpoints and the step size allowed the capacitance versus the approximate distance from the metal surface to be plotted. The results of this experiment are displayed in Figure 5. Note, all capacitance versus distance plots appearing in this thesis are representative of the typical response recorded for a minimum of ten experiments.

Results and Capacitance Model

The results, shown in Figure 5, do not coincide with the theory proposed by Equation 2 for a point charge above a conducting plane. Instead, the results seem to follow the parallel plate capacitor model:[3,4]

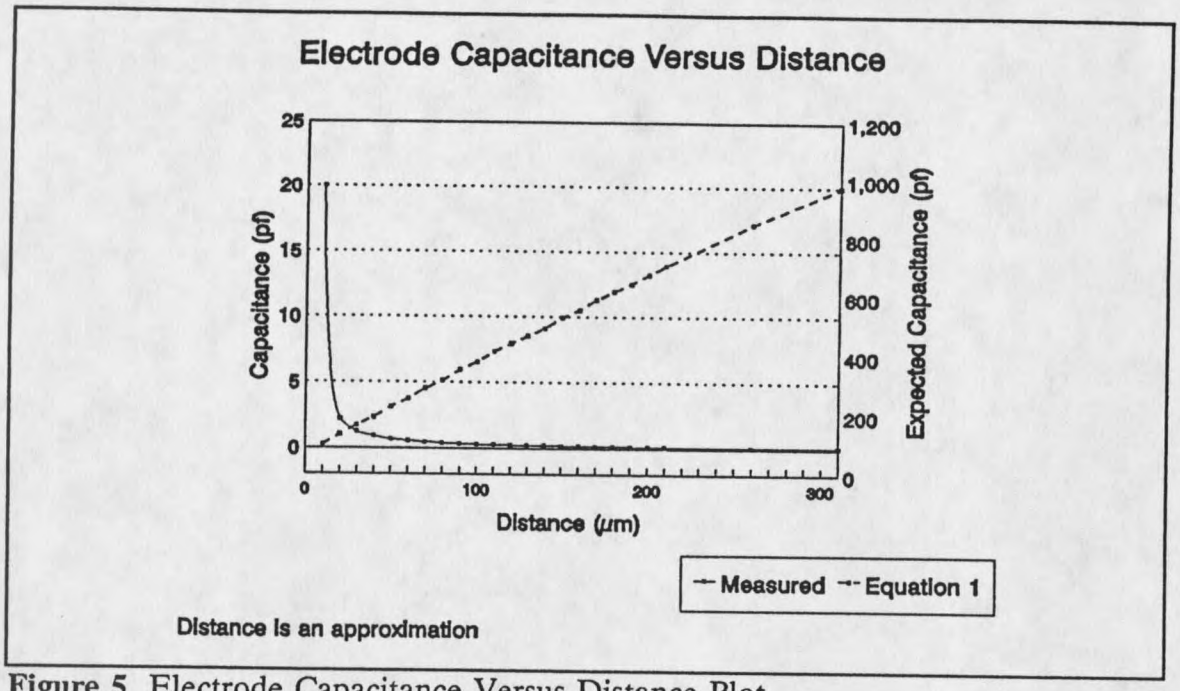

Figure 5 Electrode Capacitance Versus Distance Plot

$$C = \frac{\epsilon_o \epsilon_r A}{D} \tag{2}$$

where C is the capacitance, ϵ_o is the permittivity of free space, ϵ_r is the relative dielectric constant, A is the cross sectional area, and D is the distance between the plates. This equation is the basis of the second theory used to explain the relationship between distance and capacitance. Using the parallel plate capacitor model, a plot of one over capacitance versus distance should give a positively sloped straight line passing near the origin because of the inverse relationship between C and D. As can be seen from Figure 6, the measured data closely follows the model.

After a system model had been determined, the next step was to interactively measure the distance between the probe and the metal surface. One method for

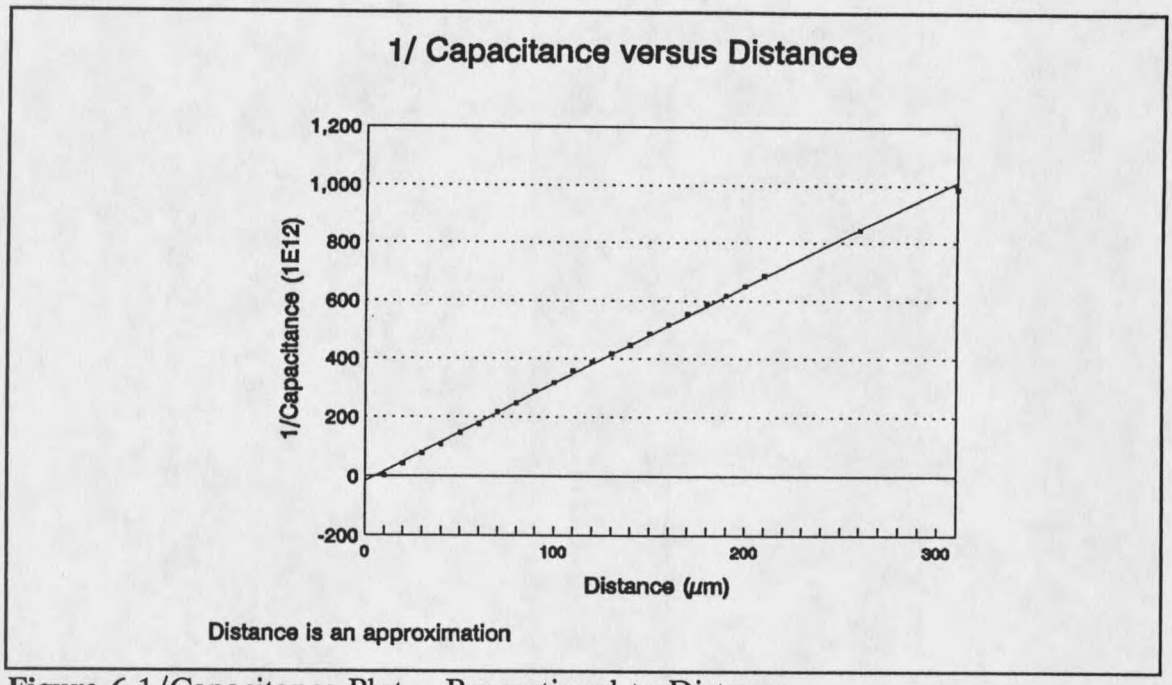

Figure 6 1/Capacitance Plot -- Proportional to Distance --

determining this distance is by using the derivative property of functions with the form f(x) = 1/x. This operation on the parallel plate capacitor model is shown in Equation 3.

$$\frac{dC}{dD} = \frac{d\left(\frac{\epsilon A}{D}\right)}{dD} = -\frac{\epsilon A}{D^2} = -\frac{C}{D} \qquad (3)$$

Factoring out C, collecting like terms, and exchanging the derivative symbol with the delta symbol, Equation 3 becomes:

$$\frac{\Delta C}{C} = -\frac{\Delta D}{D} \qquad (4)$$

This equation allows the surface distance to be determined if the capacitance is measured at two points, D_1 and D_2, to give a value of C_1 and C_2. Now, a simple algebraic calculation allows the distance to be calculated interactively.

The theory provided in Equation 4 shows that as D gets smaller for a constant ΔD, $\Delta C/C$ gets larger in magnitude thus causing the accuracy of the system to increase. Therefore, distances determined close to the metal surface should have a higher accuracy, which will allow points farther away from the surface to be resolved using the XYZ positioner. The computer positioning system allowed for electrode placement at any location in a 25 millimeter (mm) vertical plane with an accuracy of 4 μm. Therefore, the resolution of the entire setup rested on the accuracy of Equation 4 to predict the distance to the interface.

An experiment was devised to test the accuracy and resolution of the system using Equation 4. The configuration shown in Figure 4 was used once again to execute the measurements; however, the Keithley Model 3322 capacitance meter was used instead of the HP 4800A Vector Impedance meter because of its superior accuracy and resolution. To begin, the electrode was positioned at approximately 200 μm above the surface and was then lowered in 5 μm increments, with the capacitance being measured at each interval until the electrode touched the coupon. Note, the approximate distance was again determined for each step interval using the method discussed previously and was compared with the calculated distance to analyze differences between the two. Throughout a series of experiments the distance varied between 50 and 100 μm, which is not very promising considering the dimensions of

the system.

There are three major reasons why the calculation using Equation 4 varied so dramatically over the series of experiments. The first reason is attributed to the magnitude of the system capacitance. This value is small, on the order of 0.01 - 20 picofarads (pf), which is approximately the same size as the stray capacitance. Even with the Keithley instrument's option of zeroing out the lead capacitance, the connection capacitance is still significant which leads to experimental errors. The second reason deals with the quality factor (Q) of the system. Basically, the quality factor reveals how lossy a system is, because the lower the Q value the higher the losses in the system. The electrode system capacitance has a Q less than one, while a majority of good capacitors have Q's which are much greater than one. The accuracy of the capacitance measurement is proportional to the Q of the capacitor,[5] and since the Q of the circuit is so low, the accuracy of the measurements is also low. Note, the quality factor is discussed in greater detail in Chapter 5. The third error component is due to the electrical double layer which adds capacitance in series with the electrode capacitance. This concept is also discussed in greater detail in Chapter 5. Trying to resolve dimensions less than 10 μm is difficult when the size of these three error components is considered. This led to the development of the method discussed in Chapter 3.

Chapter 3

DISK CAPACITANCE

The second method in determining the distance to the surface was based on attaching a metal disk an electrode. The purpose of the disk was to increase the effective cross sectional area of the condenser plate, which causes an equivalent increase in capacitance by the direct relationship shown in Equation 2. This increases the actual plate capacitance so that it is much greater than the stray capacitance, which made the effects due to the stray capacitance negligible. Figure 7 displays a picture of this electrode-disk configuration.

The expected increase in capacitance can be determined by calculating the approximate gain in surface area between the electrode and the disk configurations. The circular surface area for both devices can be calculated using this equation:

$$A = \pi R^2 = \frac{\pi}{4} d^2 \qquad (5)$$

where A is the surface area, R is the radius, and d is the diameter of the disk. Knowing that the average diameter for an electrode is $\approx$ 15 μm and the disk diameter is 1.2 cm., yields surface areas of 0.2 square nanometers (nm) and 1.1 μm square nm, respectively. This is a difference of four orders of magnitude, which means that the disk capacitance should be four orders of magnitude greater than the

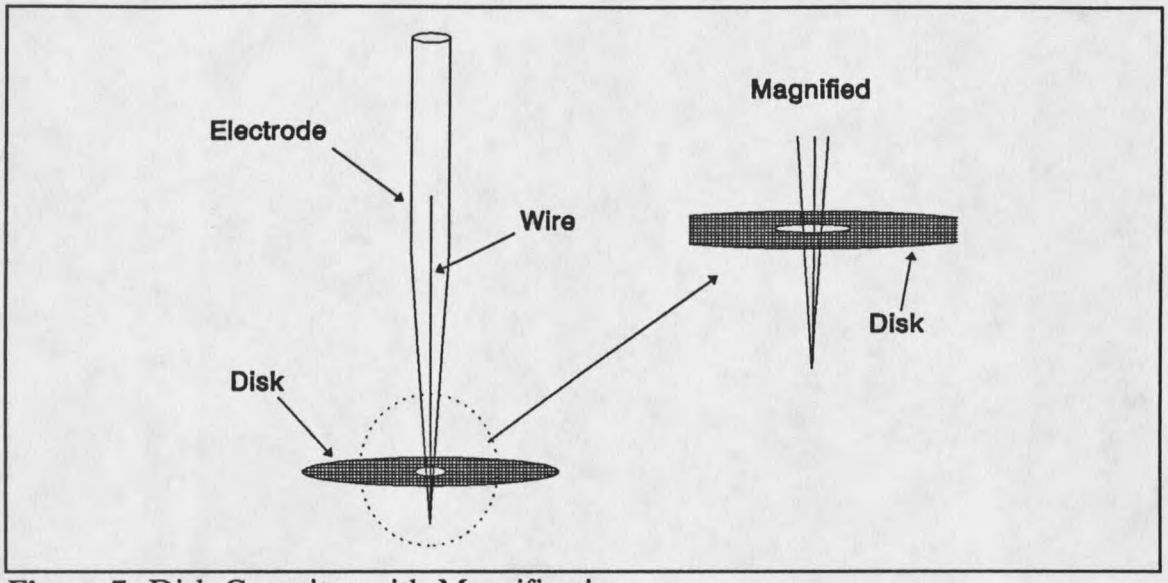

Figure 7 Disk Capacitor with Magnification

electrode capacitance. This was verified by comparing the electrode capacitance, determined from Figure 8 to the measured value of the disk capacitance at approximately 50 μm above the interface. The electrode capacitance was approximately 0.42 picofarad (pf), which when multiplied by 10^4 results in an expected disk capacitance of 4.2 nanofarad (nf). The measured value of the disk capacitance, determined by using the reactor setup displayed in Figure 4, was 3.5 nf. These results show that the disk capacitance values are in the upper nanofarad ranges, which is much greater than the stray picofarad capacitances. Therefore, the effects due to stray capacitance will be minimized, particularly at small distances (high capacitance).

Basic Disk Experimental

The capacitance versus approximate distance was measured so that the calculated distance, using Equation 3, could be compared. This was done using the same setup shown in Figure 4 except that a metal disk, with diameter 1.2 cm., was attached to a glass tube instead of an electrode. The electrode was not used in this experiment because the tip extended beyond the disk (Figure 7). A glass tube was glued to one side of the disk so that the distance could be determined in the same manner utilized in Chapter 2, with the impedance shorting to zero when the disks touched. To start, the disk was positioned approximately 50 μm above the metal surface to allow a hypothetical distance for the electrode extension beyond the disk. The results of this experiment are shown in Figure 8 along with the expected capacitance values using Equation 2.

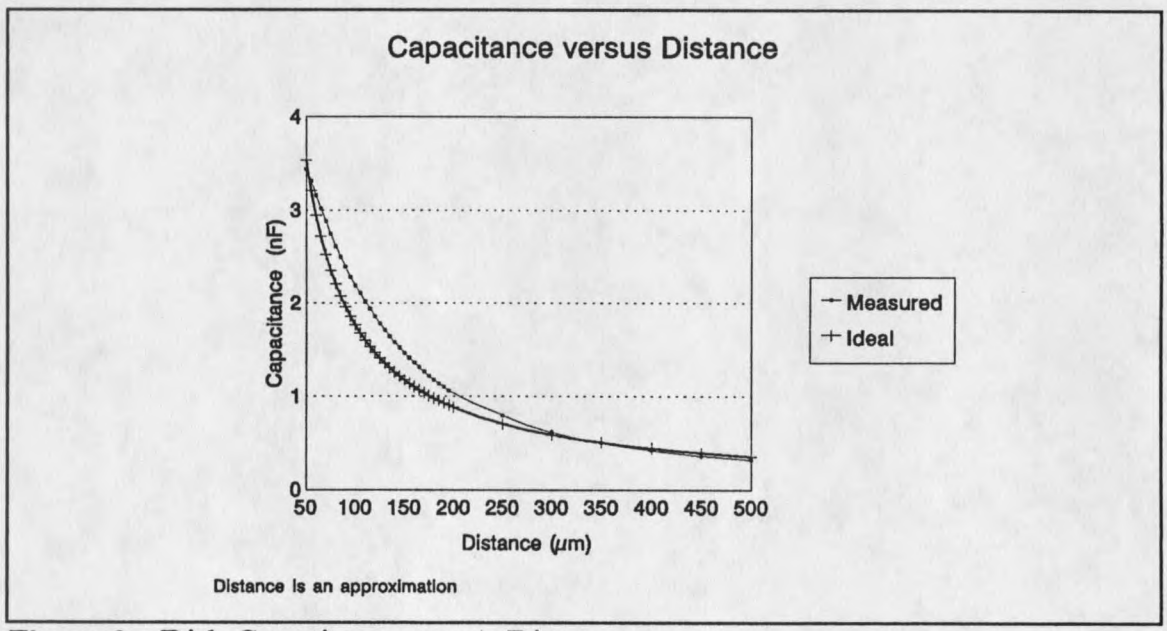

Figure 8 Disk Capacitance versus Distance

Although Figure 8 shows that the measured capacitance is close to the theoretical formula, there is some deviation. This deviation is due to fringing of the electric field at the edges of the parallel plates.[3,4,6] The derivation of the ideal parallel plate capacitor model is based on the assumptions that the electric field is uniformly distributed between the plates and the effects due to fringing are small and, therefore, can be ignored.[4,7] Figure 9 shows a graphical field plot of the fringing that occurs for a parallel plate capacitor.

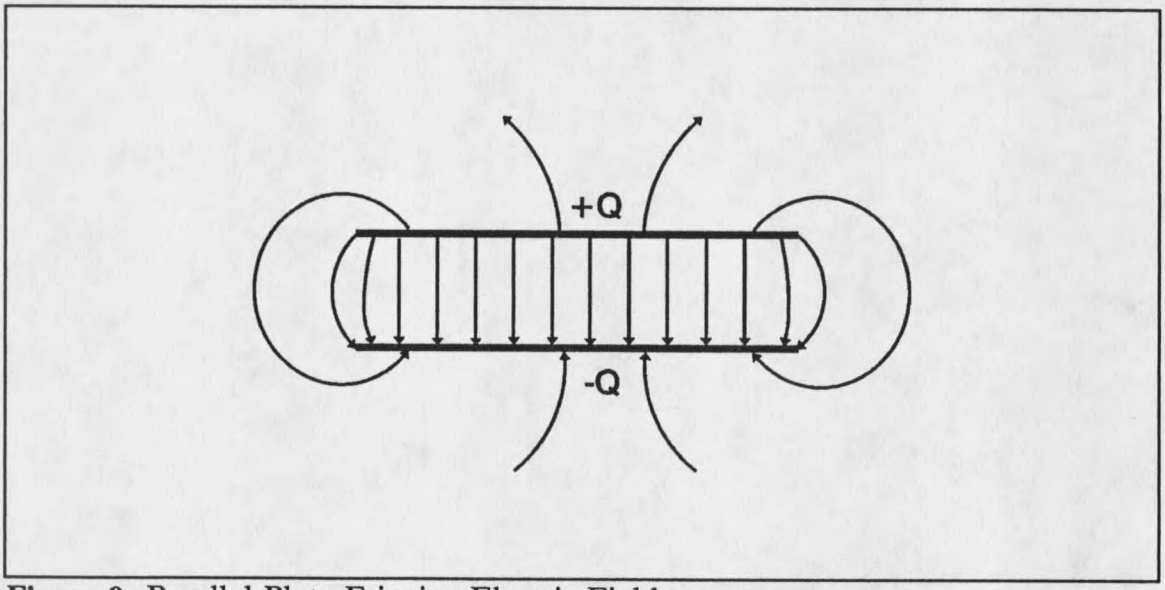

Figure 9 Parallel Plate Fringing Electric Field

As can be seen, the majority of the field appears uniformly between the plates; however, there is distortion near the edges. Many papers have dealt with the derivation of a non-ideal parallel plate condenser model which takes into account the fringing field. For example, Scott and Curtis[7] use works by Goustouv Kirchhoff[8] and J. W. Nicholson[9] to account for fringing effects in the determination of dielectric

constants using the capacitive method. The ideal parallel plate capacitor model in their paper is:

$$C_n = \frac{1.113 d^2}{16 b}\ pf \Rightarrow \frac{\epsilon_o \epsilon_r A}{D} \tag{6}$$

where C_n is the ideal capacitance, d is the diameter disk in centimeters, and b is the distance between the inner faces of the disks in centimeters. A slight compensation factor can then be added to Equation 6 to take into account the fringing field effects for a condenser consisting of one small disk and a larger disk. This modified equation is:[7]

$$C_e = 1.113 \frac{d}{4\pi}\left[\ln\frac{4\pi d}{b} - 3 + z\right] pf$$
$$\text{where}\quad z = \left(1+\frac{t}{2b}\right)\ln\left(1+\frac{t}{2b}\right) - \frac{t}{2b}\ln\frac{t}{2b} \tag{7}$$

where C_e is the non-ideal capacitance fringing factor, and t is the thickness of the disk. The final capacitance value is then calculated by taking the sum of Equations 6 and 7 and multiplying by ϵ_r.

$$C = \epsilon_r (C_n + C_e) \tag{8}$$

Scott and Curtis concluded that the use of very thin disks would help decrease their errors due to fringing to less than 1.0 percent. Note, if the disk thickness (t) is much less than the distance between the disks (b), then the z term in Equation 7 converges to zero. Because of this, the disks were made as thin as possible with nominal

thicknesses of 5-20 μm. This was accomplished by laying out the circular disks on a single sided PC-Board with the thinnest film size available. The construction of the disks in this manner was advantageous because the disk diameter was easily controlled, was light weight yet sturdy, and the thickness was minimized. The measured capacitance shown in Figure 8 is plotted again in Figure 10 along with the calculated value using Equation 8.

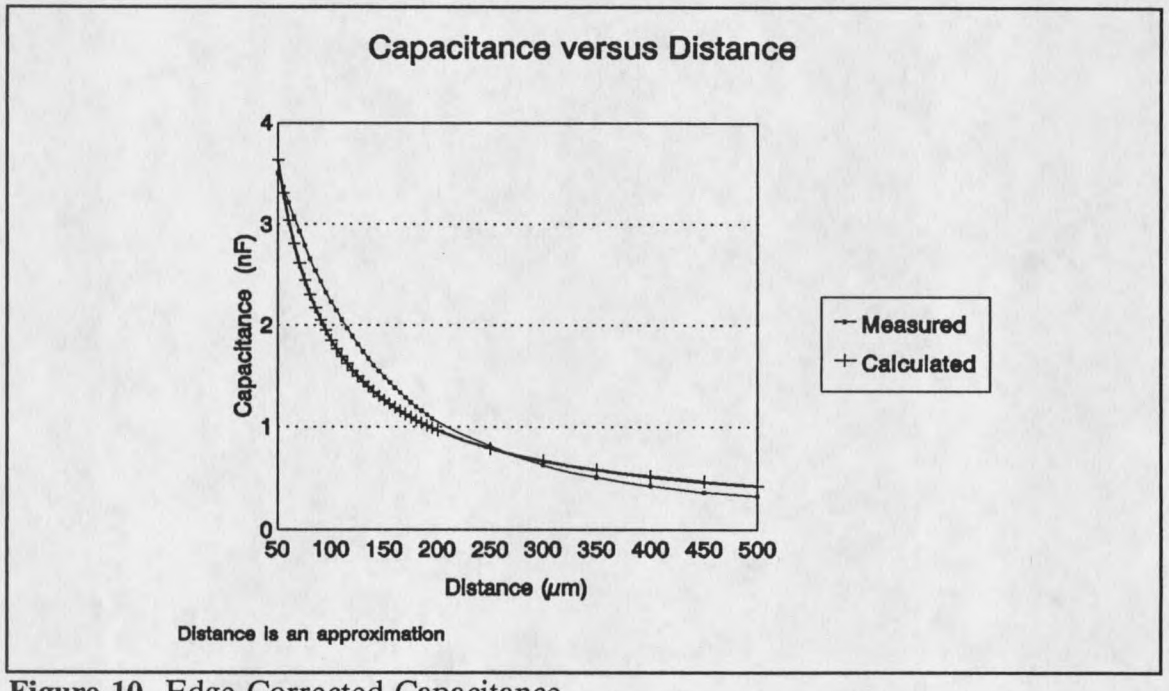

Figure 10 Edge Corrected Capacitance

At an approximate distance of 75 μm the measured capacitance had a percent deviation of 14.2% for the ideal model and 10.8% for the fringing model. Although the fringing model decreases the error between the calculated and the measured results, the errors are still too large to resolve distances less than 10 μm.

The next procedure used to compensate for fringing field was the guard ring configuration shown by the cross section in Figure 11.

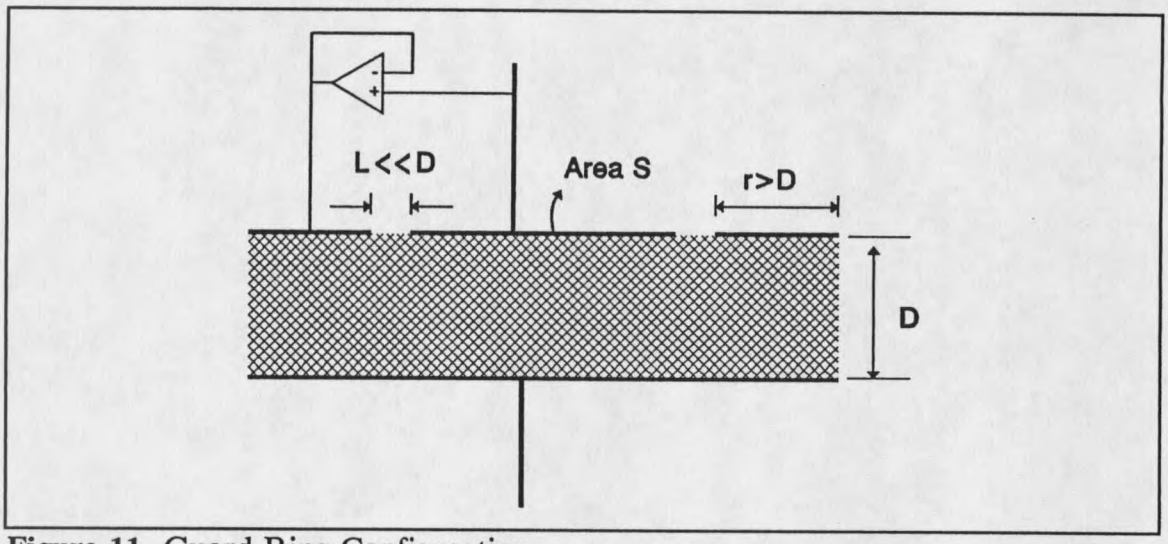

Figure 11 Guard Ring Configuration

The guard ring worked by keeping the sensing disk and the circular guard ring at the same potential, which decreases the fringing near the edge of the sensing disk. Because the two disks are at the same potential, the electric field is more uniformly distributed throughout allowing the system to approach the ideal parallel plate capacitor.[3,6,7] The best results are obtained when the distance between the guard and sensing disk (L) is much, much less than (< <) the distance between the condenser plates (D), and the width of one side of the guard ring (r) is much, much greater than (> >) D.[3,6] To correct for the edge effects due to the finite gab L, d was replaced with d+L in Equation 6, where d and L are in centimeters.[7] An operational amplifier (op amp) connected as a voltage follower allows the guard ring to be kept

at the same potential as the sensing disk, while keeping the capacitance due to the guard ring from being measured. The voltage follower acts as a high input impedance buffer with a nominal capacitance value of $\approx$ 2 pf that is in parallel with the sensing disk.[10,11] Knowing capacitors add in parallel like resistors in series[12] means that only 2 pf of capacitance will be added to the measured capacitance. This produces a 0.2% error in a 1 nf measurement. Note, Scott and Curtis reported errors less than 1% for their experiments using the guard ring technique.

An experiment was designed to test the guard ring method. First, a guard ring electrode was constructed using the PC-Board design discussed previously. The diameter of the sensing disk was kept at 1.2 cm., with r of the guard ring approximately 0.3 cm., and a width, L, of approximately 10 μm. The width, L, did not exactly meet the required specifications described in the previous guidelines. However, this width was allowed because the disk would have to be placed a minimum of 50 μm above the metal coupon to allow room for the electrode to extend past the disk. A factor of five, between D and L, was considered large enough in this experiment to allow the concept of the guard ring to be tested. Because of this, the results of the measured capacitance would be expected to have a slightly higher value than the ideal capacitance model would predict, particularly at small distances, D $<$100 μm. The guarded capacitance was measured using the same methods described previously. The results of this experiment appear graphically in Figure 12. As expected, the measured capacitance is slightly larger than the theoretically calculated capacitance, particularly at distances close to the L.

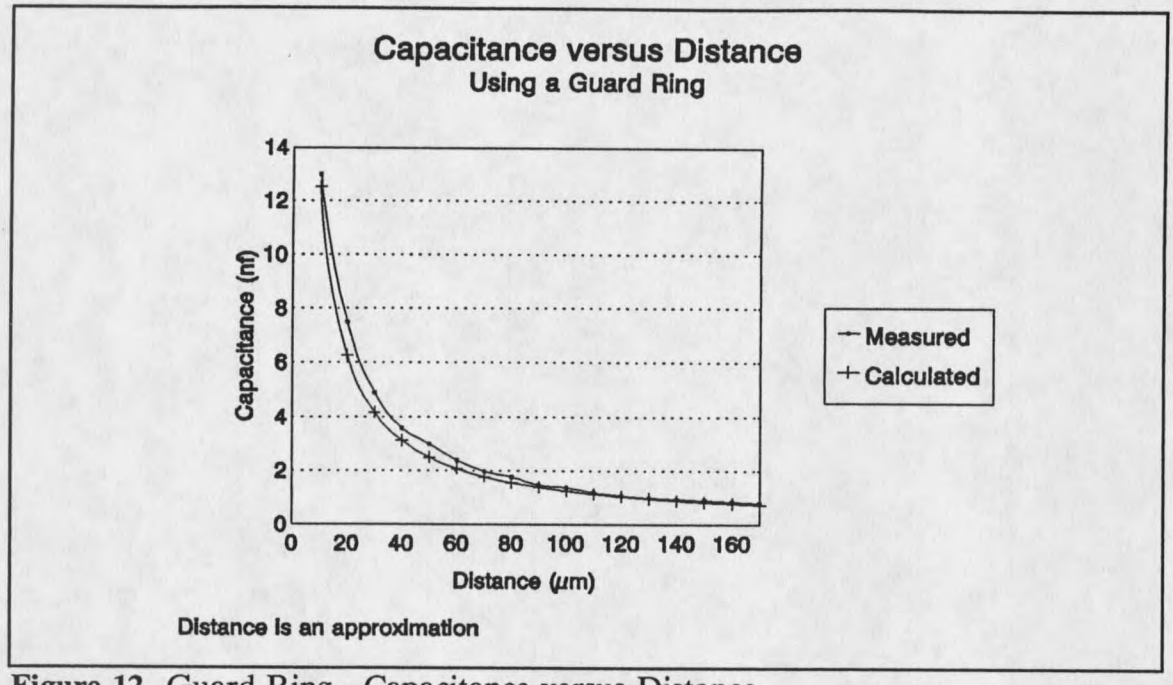

Figure 12 Guard Ring - Capacitance versus Distance

The percentage deviation between the theoretical and the measured values at a distance of 70 μm is 13.0%. Even accounting for the errors introduced by having L $\approx$ D, 13.0% is still well beyond the required accuracy needed to resolve distances less than 10 μm.

Throughout all of the disk capacitance experiments, a drifting phenomenon was noticed. Placing the disk at a constant distance above the metal surface and monitoring the capacitance versus time resulted in a slow capacitance increase over time. The reasons for this drifting are discussed in detail in Chapter 5. Because the elements associated with the drifting capacitance were so complex the capacitor methods for determining distances were no longer pursued because of practical constraints. These constraints will become clear in reading Chapter 5.

Chapter 4

SHORT CIRCUIT RESISTANCE

The third method is based on the short circuit resistance which occurs when the metal coupon and a small diameter wire contact each another. Recording the 3-D location where the resistance converges to zero at three points on the coupon, allows the plane of the coupon to be defined. The validation of this method rests on two key assumptions. The first is that the metal coupon is flat within +/- 5 μm over the entire surface, and the second is that the area of chemical interest is located towards the center of the coupon. Both the assumptions and the methods used to develop this technique are discussed.

Assumptions

The metal coupons used in the experiments were Metal Samples Company coupons with the following specifications: the diameter is 1.6 cm., thickness equals 1.06 mm, and were flat to within 30 μm. The metal coupons used were stainless steel (SS), mild steel (MS) and copper (Cu), each having approximately the same specifications described above. Each coupon was sanded and polished using 400 and 600 grit wet/dry sandpaper which helps to decrease surface deviations to less than +/- 5 μm and ensure that positive deformities would be eliminated. The elimination

of all positive deformities was needed to ensure that the electrode would not touch the metal which might cause damage to the electrode and/or the surface. Positive and negative distances are defined in relationship to the metal surface as shown in Figure 13, where the actual coupon plane is defined to be at distance equals zero.

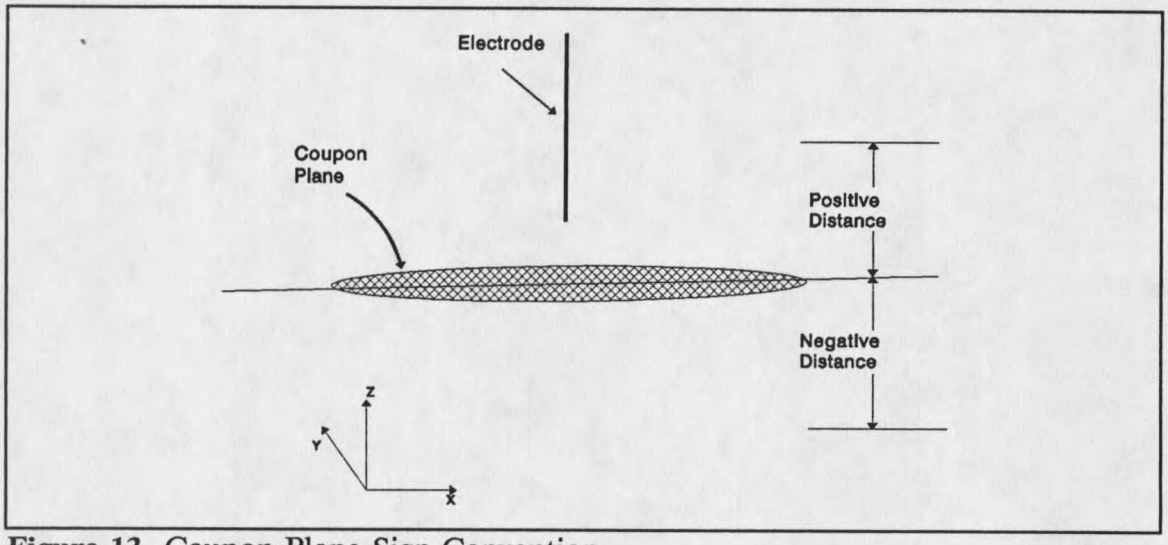

Figure 13 Coupon Plane Sign Convention

Because of the tight specifications and surface polishing, the assumption that the coupon was flat to +/- 5 μm was considered valid.

Accurate studies of biofilms near the water-metal interface dictates that only the interaction at the interface be analyzed and not the effects due to the physical edges of the coupon.[13] One of the major effects introduced near the edge of the coupon is crevice corrosion, which appears at the point where the metal and plastic holder make contact. Crevice corrosion is very dominant and can significantly disrupt the chemistry at the surface if allowed in the interface region.[13] Therefore, it is safe

to assume that the majority of the biofilm and/or corrosive region must lie towards the center of the coupon. Because of this, the wire making contact at the three points near the edge of the coupon does not seriously affect the central interface region. If this assumption holds, the non-destructive requirement of this thesis is met. Note, the three points are needed to define the metal coupon plane.

Zero Impedance Configuration

The system was designed in the same manner as discussed in Chapter 2 with the reactor setup shown in Figure 4 only slightly modified to incorporate the needs of the new method. First, the HP Vector Impedance Meter was replaced by a Keithley model 617 electrometer which was configured to operate in the resistance mode. This decision was based on the electrometer's high input impedance, analog output, and smaller size. Second, the electrode was slightly modified to allow the platinum wire to extend beyond the glass by approximately one cm.. This distance was needed to allow the wire to have enough flexibility so that it would return to its original shape after the metal surface was touched. Note, at this time the wire was not attached to the outside of an actual electrode because doing so is only a matter of mechanics and does not significantly alter the techniques or the results.

The determination of the coupon plane was done using the Micro Kinetics XYZ positioner controlled by software that allowed the system to be automated. The procedure is started by having the user input the approximate size of the area to be analyzed. Note, the scan area is a rectangle with length l and width w. The

user then positions the electrode just outside the upper left hand corner of the measurement area. This placement defines point one which then allows the computer to determine where to optimally place the other two points as related to the scanning area defined by l and w. The electrode is then lowered towards the metal surface in increments defined by the user. The increment size used in the majority of these experiments was 5 μm because this size is large enough to be time effective and small enough so that the wire is not damaged by being forced against the metal surface. After each step the computer would poll the electrometer to see if the resistance had decreased enough to show contact had been made. When contact would occur, the computer then raises the electrode one step size, 5 μm in the typical case, plus 10 μm. The additional upward step of 10 μm is used to negate any possible hysteresis effects in the positioning motor. The computer then lowers the electrode towards the surface in increments of 1 μm until contact is again detected. Note, at this contact point the resistance usually does not converge completely to zero, but it does change three orders of magnitude which allows for easy detection. The electrode is then raised 1 μm, and the computer sets this point as the 3-D origin defined by the point (0,0,0). As a reference point the XYZ positioning system defines the (0,0,0) point as "home" with all other movements related to this point. The electrode is raised 1 μm to allow a 1 micron buffer between the calculated plane and the measured plane for better protection of the electrode tip. The protection of the electrode is much more important than the accuracy loss of 1 μm. The computer then moves to point number two and performs

the same operation to determine the contact distance. This X-Y position and the Z-distance plus the one μm buffer is set to the 3-D point defined by (x_2, y_2, z_2). The third point is also defined in the same manner with its 3-D location at (x_3, y_3, z_3). Figure 14 shows how the system looks from a topological viewpoint.

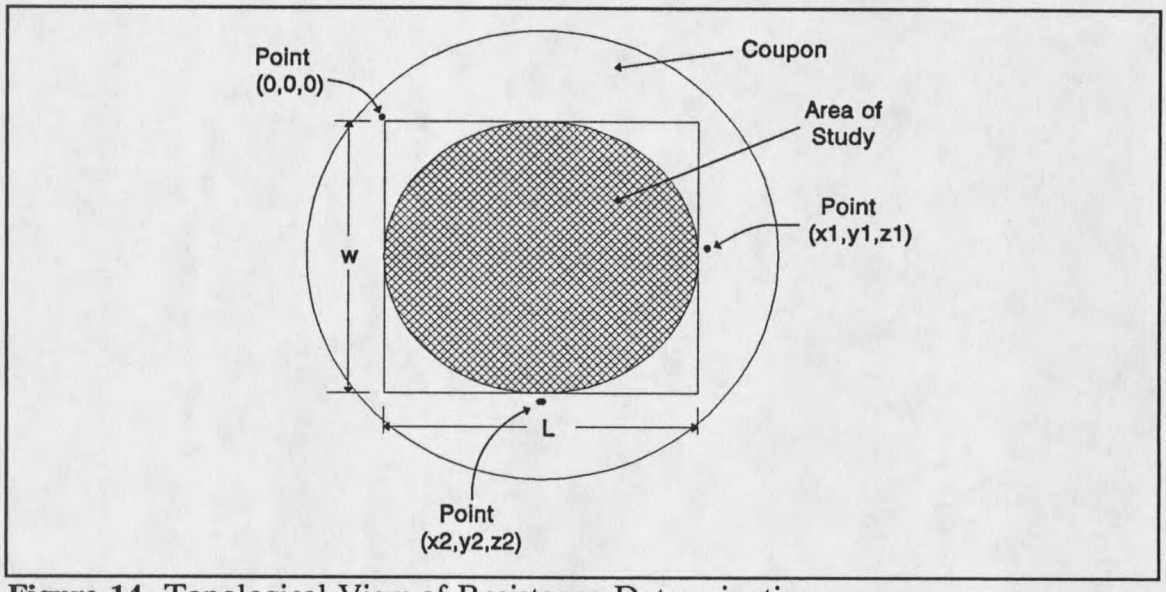

Figure 14 Topological View of Resistance Determination

The three points can now be manipulated into line segments or vectors which lie in the coupon plane. The first vectors can be obtained by subtracting the second contact point from the first to give vector v_1. The second vector can be obtained in the same manner by subtracting the third point from the first to give vector v_2. Because the first contact point is defined to be the origin, the two vectors simply equal the values at points two and three. Taking the cross product of the two vectors, v_1 and v_1, defines the normal vector, which is also the equation of the plane.[14] The cross product operation is defined by:

$$v_1 \times v_2 = \begin{vmatrix} i & j & k \\ x_2 & y_2 & z_2 \\ x_3 & y_3 & z_3 \end{vmatrix} \quad (9)$$

where x_2, y_2, and z_2 correspond to point two and x_3, y_3, and z_3 correspond to point three. The results of the cross product operation is

$$Mx + Ny + Oz = P \quad (10)$$

where M, N and O are the coefficients defined by the resultant normal vector determined from Equation 9. The value of P is determined by picking one of the three contact points, substituting the values for x,y, and z into Equation 10 and solving for P. Using the first contact point at (0,0,0), it is easy to see that P must always be equal to zero for a plane with one point at the origin. After the equation of the plane has been defined, the distance to the surface can be calculated at any positioner defined X-Y coordinate point.

Experimental

The assumptions and the methods were tested by running an experiment over a stainless steel coupon. First, the relative accuracy of the experiment was considered and steps were taken to preserve it. A special table was explicitly designed to reduce vibration error. The reactor was also secured to the X-Y table to ensure that it did not move and produce errors once the experiment had started. Second, the system was setup as if to scan an arbitrary area with dimensions 6,000 μm by 6,000 μm. The electrode was then connected to the electrometer and

positioned at the upper left hand corner of the coupon. During the determination of the coupon plane it was recorded that the pre-contact resistance was approximately 1.9 mega-ohms (MΩ) and decreased sharply to roughly 8 kilo-ohms (KΩ) when contact occurred. After the computer had determined the equation of the plane the electrode was moved to a random point on the coupon. From this random point, a 1000 μm by 1000 μm grid was analyzed to test the resolution and accuracy of the distance calculation. The XYZ positioning table was then used to scan the grid in 100 μm increments with the short circuit contact point being recorded. This measured point (d_m) was then compared to the expected distance (d_e) determined by using the plane equation and the difference (d_e-d_m) was recorded. Note, using 100 μm increments allowed for 121 points to be analyzed (10 points plus the zero point).

Results

The maximum and minimum deviation (d_e-d_m) in all 121 points was +2 μm and -4 μm, respectively. A 3-D surface plot of the data obtained from this experiment appears in Appendix B. This plot allows the assumption stating that the surface was smooth to within +/-5 μm to be verified. An imaginary plane is drawn through this plot at minus 1 μm to indicate where the actual coupon plane occurs without the 1 μm buffer. This plot shows that the surface has a small valley of roughly 3 μm in depth which is surrounded by ridges that extend 2 μm high. Because

the 3 μm valley extends gradually over 600 μm it would not be readily detectable by human eye or optical microscope.

Errors and Resolution

Although precautions were taken to eliminate errors due to vibration, there were still vibration problems. When the probe was placed at a distance 1 μm above the contact point, it was observed that people walking by or machinery turning on and off caused contact to be made. This means that the resolution of the system is at best greater than 1 μm. This coupled with errors in the positioning system are easily enough to raise the value to 2 μm.[15] Assigning the 2 μm errors to the plot still allows the initial assumption of surface flatness to hold, except for one point that was at -4 +/- 2 μm.

Reactor Construction

The reactor and the coupon holders were professionally machined in hopes that the coupon would be completely parallel to the positioner X-Y plane. The short circuit method allowed the results of this extra precaution to be analyzed. In the 1000 x 1000 μm grid discussed previously, the tilt of the coupon was such that the (0,0) point on the X-Y plane corner was 19 μm lower than the lower right hand corner at point (1000,1000). The tilt of the entire coupon was measured to be 124 μm across the coupon from the highest to the lowest edges. Other machined coupons that were tested displayed a tilt which range between a minimum of 73 μm

and a maximum of 248 μm. These results clearly show that the coupons are significantly tilted. This means scans using ion-selective electrodes at a level parallel to the X-Y plane measure ion concentration at distances that may vary as much as 250 μm relative to the actual metal surface which can seriously bias the data taken in an experiment. This can be easily seen by studying the dissolved oxygen (DO) profiles through a thick biofilm (see Figure 1). The dissolved oxygen concentration tends to be directly proportional with the distance to the interface. Knowing this, it can be easily seen how two different points in the X-Y plane might give different DO readings. However, this variation is based on differences in distance and not deviations in the biofilm structure itself. This analysis clearly shows the need for an accurate determination of the distance between the metal surface and the electrode tip.

Chapter 5

TEMPERATURE VARIATIONS

Temperature fluctuations have a significant effect on the capacitor system. Slight increases in temperature can cause the measured capacitance value to vary as much as one percent depending on temperature swings in the bulk solution. Measuring capacitance using the disk method of chapter 3 showed that as the temperature increased, the measured capacitance also increased. This is very unusual because ϵ_r for water has a negative temperature coefficient[16,17,18] which means as the temperature increases the capacitance should decrease. The reason for this discrepancy stems from the electrical double layer formed at the metal surface.[19,20,21] The theory behind the negative temperature coefficient of ϵ_r and the electrical double layer as well as how they affect the distance determination methods is discussed in detail.

Dielectric Constant of Water

The relative dielectric constant for materials is defined by four polarization properties; electronic, ionic, orientational, and space charge.[16,17,18,22] The polarization (**P**) of a material is related to the dielectric constant by:[4]

$$P = \epsilon_o(\epsilon_r - 1)E \tag{11}$$

where **E** is the electric field. Substituting the four polarization components into Equation 11 and solving allows ϵ_r to be determined.

$$\epsilon_r = 1 + \frac{1}{E\epsilon_o}\left(+P_{\text{electronic}} + P_{\text{ionic}} + P_{\text{orientational}} + P_{\text{space charge}}\right)$$

$$\epsilon_r = 1 + \left[\frac{N_a\alpha_e}{\epsilon_o}\right] + \left[\frac{N_i\alpha_i}{\epsilon_o}\right] + \left[\frac{N_p p^2}{3\epsilon_o kT}\right] + \left[\frac{F(1/T,\omega,material)}{\epsilon_o}\right] \tag{12}$$

where N_a is the atoms/volume having a dipole moment, α_e is the electronic polarizability, N_i is the ionic molecules/volume having a induced dipole moment, α_i is the ionic polarizability, N_p is the number of polar molecules/volume, p is the average dipole, k is Boltzmann's constant, and T is temperature. The last term, space charge polarization, is a function of material, temperature, and frequency (ω). The third term in Equation 12, which applies only to polar molecules like water, is the most important when considering temperature fluctuations of ϵ_r. This term clearly shows that as temperature increases, the dielectric constant should decrease for polar molecules. The actual relationship between temperature and ϵ_r for water is given by Wyman's Equation:[17]

$$\epsilon_r = 87.740 - 0.4008T + 9.398(10^{-4})T^2 + 1.410(10^{-6})T^3 \tag{13}$$

where T is the temperature in degrees celsius (°C). This equation shows that at temperatures near 25 °C, ϵ_r decreases with increasing temperature. Since the capacitance is directly related to ϵ_r, one would expect that as the temperature of the water increased, the measured capacitance would decrease accordingly. This, however, was not the case determined in experiments where the distances between the plates were on the order of micrometers. The reason for this lies in a phenomenon known as the electrical double layer.

Electric Double Layer

The electric double layer is broken up into two components, the Helmholtz region and the Gouy-Chapman region.[19,20,21] The Helmholtz region is based on the fact that the electrode (disk) is a good conductor, which means at equilibrium any free charge will distribute itself on the surface in such a manner as to keep the internal **E** field equal to zero.[4,19] Helmholtz proposed that the solution's excess counter-charge must also build up near the electrode surface so that the net charge equalled zero and the system remained in equilibrium. The name, double layer, stems from these two oppositely charged planes which are separated by a distance in the order of angstroms.

The Gouy-Chapman model describes how the overall thickness of the double layer can change with varying electrolyte concentrations and applied potential. One can readily see that if the electrolyte is relatively low in charge carrier density, the thickness of the double layer must increase to allow the surface charge to be

canceled. The thickness is limited due to the electrostatic attraction and repulsion of charges and the thermal process which tends to randomize the layer.[19] Because of this, the Gouy-Chapman region is classified as the diffuse layer, where the major concentration of charge is located near the surface because the electrostatic forces are large enough to overcome the thermal agitation. As the distance increases, the charge concentration decreases because the thermal agitation overcomes the lower electrostatic forces. The average thickness of this layer can be inserted into Equation 2 to approximate the capacitance of the system. Note, the diffuse layer for a water electrolyte can be on the order of micrometers in thickness.[21] A better model of the capacitance for both the Helmholtz and the diffuse layer is shown in Equation 14. This model uses the Stern Modification which takes into account the ion size, where the Gouy-Chapman model assumes the ions to be point charges.[19] The results are:

$$\frac{A}{C} = \frac{x_2}{\epsilon\epsilon_o} + \frac{1}{(2\epsilon_r\epsilon_o z^2 e^2 n^0/kT)^{1/2}\cosh(ze\phi_2/2kT)} \qquad (14)$$

where A is the cross-sectional area, x_2 is the thickness of the Helmholtz layer, z is the (signed) number of units of electronic charge on ion i, e is the charge of an electron, n is the bulk concentration, k is Boltzmann's constant, T is the absolute temperature, and ϕ_2 is the electrostatic potential at x_2. Equation 14 is shown in its reciprocal form because the Helmholtz layer and the diffuse layer act as two capacitors in series. The second term in Equation 14 displays the inverse relationship between capacitance and temperature of the diffuse layer. Knowing that the capacitance is inversely proportional to the distance, it can be seen that the thickness of the diffuse

layer must increase with increasing temperature. This element now allows the positive temperature coefficient of the disk capacitance to be analyzed.

Positive Temperature Coefficient

The entire system consists of five separate dielectric regions between the plates of the capacitor. These regions are the two Helmholtz and two diffuse layers, which occur at the metal plates, and the water between these regions. This total capacitance model is shown in Figure 15.

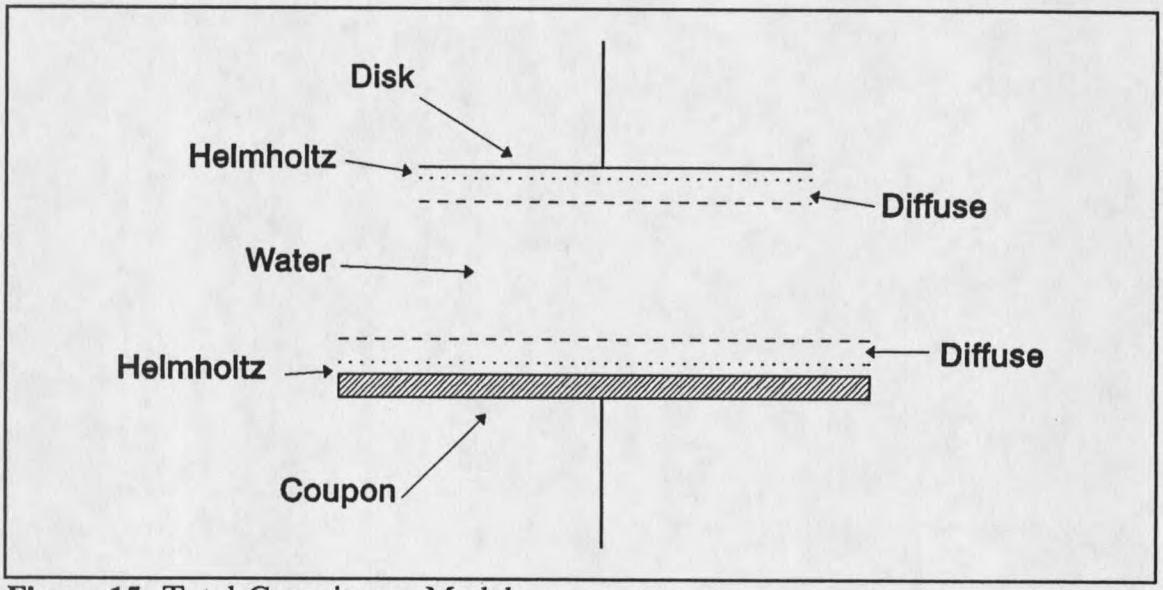

Figure 15 Total Capacitance Model

When measuring the capacitance between the two plates, the Helmholtz and diffuse layers usually have capacitance values that are much greater than the solution capacitance due to the layers' thicknesses. Because capacitors in series add as one over their reciprocals,[12] the Helmholtz and diffuse capacitances can be ignored if the

solution capacitance is small enough. In the analysis of the positive temperature coefficient it will be assumed that the additional capacitance due to the Helmholtz and diffuse region can be ignored. This assumption is not actually true for this system because the thickness of the water can be of the same order as the thickness of the diffuse region. However, the assumption does simplify the equations and allows for a more intuitive analysis. This assumption then allows the measured capacitance to be modelled by Equation 2. Taking the partial derivative of this equation gives:

$$\partial C = \frac{\epsilon_o A}{D}\partial\epsilon_r - \frac{\epsilon_o \epsilon_r A}{D^2}\partial D \qquad (15)$$

which assumes that the cross sectional area does not change. Factoring out C and changing the partials to the delta format gives:

$$\frac{\Delta C}{C} = \frac{\Delta \epsilon_r}{\epsilon_r} - \frac{\Delta D}{D} \qquad (16)$$

Knowing that ΔC has been experimentally determined to increase with temperature while $\Delta\epsilon_r$ decreases with temperature (Equation 13) means that ΔD must also decrease to preserve the equality shown in Equation 16. Because $\Delta\epsilon_r/\epsilon_r$ is small for a +/- 0.5 degree Celsius swing in temperature (≈ 0.003), ΔD can be on the order of nanometers and cause the positive swing in ΔC. This is because D is in the micrometer range which is like multiplying ΔD by a value equal to approximately 10^5. The distance between the plates for most capacitor systems is on the order of millimeters which is large enough to cause the second term in Equation 16 to

become negligible when compared to the deviations in ϵ_r. In the case where d is large, Equation 16 is reduced to the more generally known form where fluctuations in capacitance are directly caused by changes in ϵ_r.

The next part of the analysis assumes that the net distance (d_t) between the plates remains constant with temperature meaning $\Delta d_t = 0$. This is a safe assumption in this derivation because if Δd_t were to change with temperature it would only decrease due to the thermal expansion of the plates. This would only enhance the positive temperature coefficient discussed previously. As displayed in Figure 15, the total distance between the plates can be defined by:

$$d_t = 2d_{dl} + d_w \tag{17}$$

where $2d_{dl}$ is the double layer thickness of both metal surfaces and d_w is the width of the water. It has already been determined from Equation 14 that the diffuse region of the electrical double layer increases with temperature ($\Delta d_{dl} > 0$). If Δd_t equals zero, then Δd_w must decrease with temperature just as predicted by the analysis following Equation 16. In the actual system the effects due to both the diffuse layer and the thermal expansion of the plates cause the effective thickness of the water to decrease which in turn causes the measured capacitance to increase.

The Quality Factor

Analyzing the temperature variations of the water between the condenser plates is the next step in explaining the capacitance drift over time. Full understanding of this phenomenon dictates that the Q or quality factor of the system

must be addressed. The analysis of a non-ideal capacitor leads to a relationship by which the dielectric material can be modelled using complex notation in the form of A-jB. This complex dielectric constant (ϵ_r) is attributed to the facts that the polarization is unable to keep up with the electric field and the dielectric has a conductivity (σ) associated with it.[4,6] This leads to Equation 18 which displays the components that make up ϵ_r, where ϵ_o is the permittivity of free space, and ω is the radian frequency.

$$\epsilon_r = \epsilon' - j\epsilon'' \; ; \quad \epsilon'' = \left[F(material,\omega) \parallel \frac{\sigma}{\omega \epsilon_o} \right] \tag{18}$$

Knowing the impedance of a capacitor (Z_c) is:

$$Z_c = j\omega C = j\omega \epsilon_r C_o \tag{19}$$

where C_o is the vacuum capacitance, substituting Equation 18 into 19 and solving for the real and imaginary parts leads to

$$Zc = \left[\epsilon'' \omega C_o + j\epsilon' \omega C_o \right]^{-1} \tag{20}$$

Basic circuit theory allows Equation 20 to be modeled as an equivalent parallel resistor-capacitor (RC) network, with $R_{eq} = 1/(\epsilon'' \omega C_o)$ and $C_{eq} = \epsilon' C_o$. This RC network is shown in Figure 16 with a sinusoidal driving source.

The circuit element R_{eq} is referred to as the dielectric loss resistance, while C_{eq} is a basic lossless capacitor.

The development of the equivalent RC network allows the Q of the circuit to be analyzed. Q is defined in Equation 21, where K is a proportionality constant that

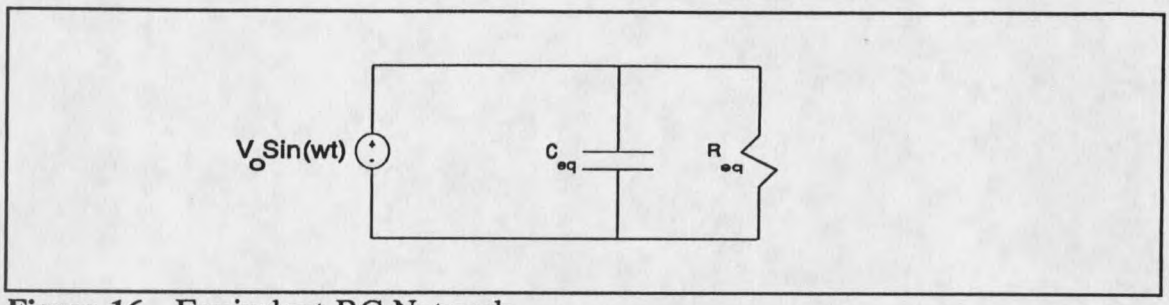

Figure 16 Equivalent RC Network

depends on the system.[12] In this case, K equals 2π because the system is in sinusoidal steady state.

$$Q = K\left\{\frac{Peak\ Energy\ Stored}{Average\ Power\ Dissipated}\right\} per\ period = \omega\frac{W_{peak}}{P_{avg}} \tag{21}$$

Under sinusoidal conditions the peak energy stored and the average power dissipated are easily calculated using Equations 22 and 23.

$$Peak\ Energy\ Stored = W_{peak} = \frac{C_{eq}V_o^{\,2}}{2} \tag{22}$$

$$Average\ Power\ Dissipated = P_{avg} = \frac{V_o^{\,2}}{2R_{eq}} \tag{23}$$

Substituting these equations into 21 produces a value of Q that is only a function of the relative dielectric constant.

$$Q = \frac{2\pi}{T}[R_{eq}][C_{eq}] = \frac{\epsilon'}{\epsilon''} \tag{24}$$

This equation clearly displays the inverse relationship between Q and ϵ" which plays a key role in analyzing temperature fluctuations between the condenser plates. The dielectric constant (ϵ') for a water based electrolyte is approximately equal to 80. This allows ϵ" to be calculated if the Q of the system is measured using a capacitance or vector impedance meter. Table 1 displays a listing on how Q varied with frequency applied and also presents a calculated value for ϵ". These values were obtained by placing the condenser disk at a constant distance above the metal surface and measuring Q at discrete frequencies from 10 KHz to 90 KHz.

Table 1 Quality factor Versus Frequency

Frequency KHz	10	20	30	40	50	60	70	80	90
Q	0.10	0.24	0.33	0.48	0.54	0.69	0.84	0.72	0.58
ϵ"	800	333	242	166	148	115	95.2	111	137

The value of ϵ" displayed in Table 1 allows the equivalent loss resistance for the disk capacitor to be determined at distances between 10 and 1000 micrometers. The determined R_{eq} values range between one kilo-ohm (KΩ) and one mega-ohm (MΩ). These values, coupled with the knowledge that a one volt sinusoidal input at 50 KHz was applied to the reactor using the Keithley model 3322 capacitance meter, allows Equation 23 to be used to calculate the average power dissipated (P_{avg}). These calculations show that the dissipated power ranged between 0.5 milliwatts (mW) and 0.5 microwatts (μW). Under normal operating conditions, this power is

dispersed into solution in the form of heat which slowly causes the temperature between the plates to increase.

The physical nature of the system is not conducive to heat dissipation. A majority of the heat produced by the capacitor occurs in the very small volume between the two capacitor plates while the bulk water temperature remains constant. In analyzing the system, the two metal plates are assumed to be at the same temperature as the bulk solution. This assumption simplifies the analysis without a significant loss in accuracy. The equivalent thermal system is shown in Figure 17. The thermal power, K, supplies a volume at temperature T1 with heat energy. This volume is considered to be surrounded by a constant temperature sink at Ts.[23] The equivalent electrical circuit is also shown in Figure 17, where the thermal power applied is a constant current source of magnitude K. The mass of the volume has the ability to store energy which can be modelled as an electrical capacitor. The mass also has a thermal resistance associated with it, modelled by an equivalent resistor.[23]

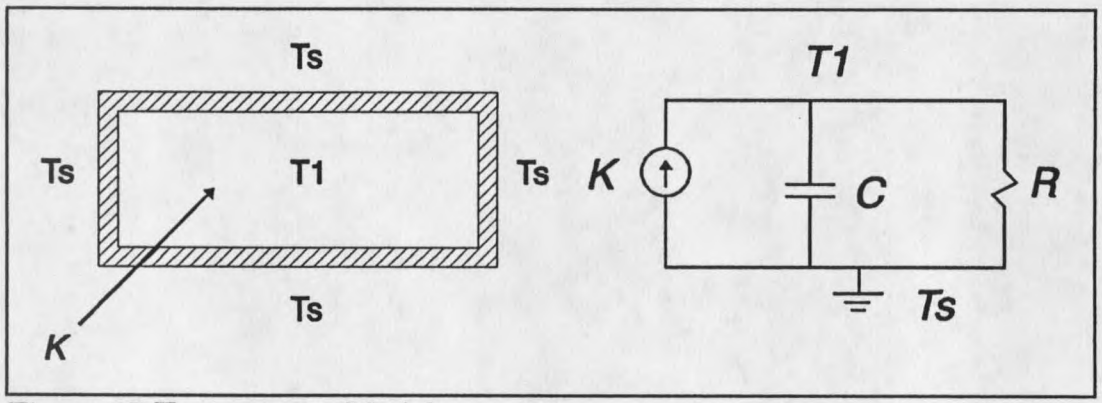

Figure 17 Temperature Model

Both system models displayed in Figure 17, whether it be from an electrical or physical point of view, show that the reactor must pass through a transient state before equilibrium is reached. Note, a complete model of the heat transfer system is not generated because there is a transient and steady state which allows the desired conclusion to be obtained. The transient and steady state portions of the system are dependent on distance, disk size, solution type, electric double layer, and temperature. Therefore, the system is quite complex and composed of a large number of interrelated variables making it difficult to model in real time. Although all of the above variables can be controlled, the loss in generality is too great thus defeating a major requirement for determining the distance to the surface.

Controlled Temperature Measurements

A constant temperature flow reactor was used to test the theory on why the capacitance increases over time at a constant distance above the surface. The system consisted of a Fisher Scientific model 9100 temperature controller feeding a flow reactor that contained a stainless steel coupon and the sensing electrode. This configuration, shown in Figure 18, allows constant temperature water to pass between the plates prohibiting increases in temperature. Experiments with this system showed that the capacitance no longer drifted over time. However, the random fluctuations (noise) caused by water moving between the plates and vibrating the electrode were significant.

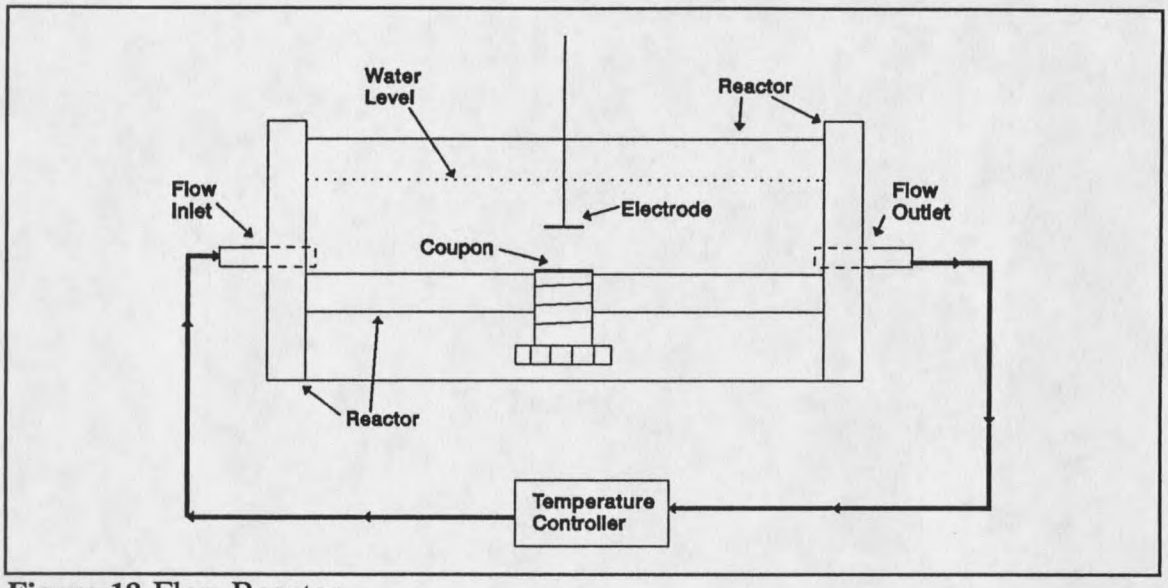

Figure 18 Flow Reactor

Although the temperature controller allowed the capacitance drift to be eliminated, the method possesses low feasibility for actual biofilm structures. Introducing a relatively high velocity flow into a biofilm structure can significantly modify the chemistry near the interfacial region. The sole purpose of this thesis is to develop a procedure that allows the biofilm to be analyzed with ion-selective electrodes without disrupting the system's natural state.

Chapter 6

ANALYSIS AND DISCUSSION

The three methods of measuring the distance between the electrode tip and the metal surface, proposed in this thesis differ considerably in respect to their configurations, accuracy, and difficulties. Of the three, the simple electrode capacitance method appears, at first, to be the best option available. The capacitance between the tip of the electrode and the metal surface can be continuously measured and analyzed in real time. It would appear to allow the electrode to be positioned with accuracy without destructively interfering with the surface or the interface chemistry. Although, this method appears good in theory, the practicality is limited. Compensating for the tip size and the non-ideal capacitance properties dictates that the measurements be taken with the electrode close to the metal surface. This introduces errors into the system due to two capacitances, stray and the electric double layer. These two capacitances can usually be ignored in systems with larger dimensions. However, when the electrode cross sectional area is small and the spacing is of the same magnitude as the double layer, the components are no longer negligible. Therefore, the accuracy needed to measure the distance between the coupon and the electrode is not available without knowing the values for the two error capacitances. The determination of these two error

capacitances is difficult at best, particularly in a natural environment such as a biofilm system.

The disk technique for measuring the distance is definitely the most difficult of the three methods. The low Q of the system decreases the accuracy at which the capacitance can be measured and allows heat to be dissipated into solution. The heat dissipation causes the temperature to increase which in turn causes the capacitance to rise due to the expanding double layer and condenser plates (see Chapter 4). Another problem that is associated with this method is attaching the disk to the electrode at a known distance from the tip. Not only must the distance between the tip and the electrode be measured accurately but the disk must be tilted at an exact angle to match the tilt in the coupon so that the two plates are parallel to one another. Although all of these components can be controlled with careful planning and preparation, the cost due to time, equipment, and accuracy is too large compared with those of the third method.

The short circuit resistance technique is the easiest and most accurate of the three methods. Extending a wire 5-10 μm beyond the tip of the electrode and measuring the 3-D point where the resistance goes to zero can be done with any precision computer controlled positioning system. By optically measuring the distance between the wire and the tip of the electrode, the distance between the tip and the metal surface can be easily determined using the equation of the plane. Experiments that were run to test the accuracy of the short circuit resistance technique showed that the maximum deviation between the expected coupon surface

and the actual surface were within the specified +/- 5 μm range. This high degree of precision should allow a biofilm and/or corrosion coupon to be accurately scanned in all three dimensions. This will allow better corrosion and biofilm models to be developed as well allowing an aid to test the validity of older models.

Future Developments

Sensing Volume

The major direction of this project will now be to determine the optimum distance each sensing electrode (pH, DO, sulfide, ...) must be in order to obtain accurate corrosion scans and biofilm profiles. Ideally, an electrode is assumed to measure at a single point because only the tip is sensitized and the size of this tip is small, as shown in Figure 2. This may be the case in theory, but in practice the electrodes actually analyze a small volume which surrounds the tip. Because of the electrode nature and this imaginary volume size, the ions under study are assumed to have a continuous distribution throughout the volume. A method that might allow the size and shape of this volume to be determined is by placing the electrode at known distances above the surface and measuring the ion concentration as the probe is moved towards the interface. This will allow the changes in concentration along with the changes in distance to be recorded. To get the volume shape, this procedure will most likely have to be done in all three dimensions. Assuming that the step size is small, less than 5 μm, the ion concentration should not change if the constant sensing volume around the electrode is large compared to the step size.

This will allow the collected data to be analyzed and a model which approximates the size and shape of the volume to be determined. After the model has been defined the optimum step size and distance above the interface can be approximated so that efficient and statistically correct biofilm profiles are obtained.

Thick Biofilms

The short circuit resistance method will have to be tested on biofilm samples which are in the range of 10 - 20 mm thick. These types of biofilms might present a problem to this method because the Z positioner will have to move over an extended range, (10 - 20 mm) which will increase the positioning errors. These types of biofilms tend to create corrosion pits and other deformities on the metal surface.[13] If, when determining the coupon plane, the metal wire hit one of these deformities, the plane equation could be seriously affected. This is one reason why the wire attached to the electrode must be so large in diameter ($\approx$ 100 μm) so that any deformities might be negated by the sheer size of wire. Future experimental results in this area will help determine if more than three points need to be taken so that an averaging operation can be performed to negate the effects due to deformities on the plane equation.

Electrode Tip Size

Measuring the cross sectional area of an electrodes tip is one area of interest in the construction of ion selective electrodes.[24] A method that might allow this cross sectional area to be determined is through the capacitance method and the use of

equation 1. A reactor could be constructed that would allow the distance between an electrode and the metal surface to be optically measured as well as having a control for temperature fluctuations. The stray capacitance as well as effects due to the electric double layer could be controlled and measured. While these values can be controlled in this reactor system, they cannot be in a biofilm reactor because the controls would disrupt the natural state of the system. Measuring the capacitance of the electrode and subtracting out the stray capacitances and double layer capacitance will allow the approximate cross sectional area to be calculated directly if the distance is known. The ultimate accuracy of this system resides in how accurate the distance can be measured, the extent to which stray and double layer capacitance can be controlled, and the fluctuations in temperature. Testing of this method would be done by comparing the results with more conventional methods for determining the tip area, such as optical microscope determination, chronopotentiometry, and chronoamperometry.[24,25,26]

Major Contribution

The major contribution of this thesis is the development of an effective method to measure the distance between the electrode tip and the metal surface in the presence of a biofilm and/or corrosion. The advantageous of this method over other methods tried is that it is fast, easy to implement, and accurate. The overall accuracy of the system depends on three main components: 1) Surface flatness 2) Accuracy of the positioning system 3) The ability of the table to dampen external

vibrations. If the error components are minimized, the electrode can be placed at any nominal 3-D location relative to the metal surface with a minimum accuracy of 5 μm, without damage to the surface or the electrode. This allows a single electrode to run more than one profile scan over the metal coupon without breaking because of surface contact.

Chapter 7

CONCLUSIONS

The measurement of the distance between the electrode tip and the metal surface was performed using three methods: 1) Electrode Capacitance 2) Disk Capacitance 3) Short Circuit Resistance. Of these three methods, the short circuit resistance technique was the easiest to use and most accurate. These conclusions, as well as a number of more general statements are listed below in tabular format.

1. The model that best fits the electrode and disk configurations is the parallel plate model where the capacitance is inversely proportional to the distance.
2. The electrode capacitance is adversely affected by stray capacitance which is of the same magnitude as the actual capacitance between the tip of the electrode and the metal surface.
3. The effects due to stray capacitance can be negated by using a disk attached to the electrode.
4. The fringing effects due to the electrode disk are large and need to be compensated for using theoretical equations and/or a guard ring configuration.

5. The disk capacitance has a positive temperature coefficient even though the relative dielectric constant (ϵ_r) has a negative temperature coefficient which usually implies that the capacitor will also have a negative temperature coefficient.
6. The thickness of the electric double layer increases with temperature. This coupled with the relatively small dimensions causes the positive temperature coefficient noticed in experiments.
7. The quality factor (Q) of the water based dielectric is low which causes power dissipation into solution. This power dissipation causes the temperature to increase which, in turn, results in a capacitance increase with temperature.
8. Attaching a disk to an electrode and accurately measuring the distance between the electrode tip and the metal disk is difficult particularly if the disk must be tilted to match the slope of the metal coupon.
9. The short circuit resistance method is easier and more accurate in determining the distance to the metal surface then the two capacitance methods tried.
10. The metal coupons are flat to within the specified +/- 5 μm over the range analyzed after being sanded and polished. This allows the short circuit resistance technique to be used.

11. The accuracy of the short circuit resistance method depends mainly on the accuracy of the positioner and the degree to which the table holding the positioner can be isolated from external vibrations.
12. The short circuit resistance method does cause some damage to the metal interface, but if the area of interest resides towards the center of the coupon the damage has no effect on the surface chemistry in the area of study.
13. The wire used to perform the short circuit should be reasonably large ($\approx 100\,\mu$m) so that it is rigid enough to return to its original shape once the metal surface has been touched.
14. The capacitance method could be used to approximate the cross sectional area of an electrode tip if effects due to stray capacitance, temperature, electric double layer, and distance can be controlled.

REFERENCES CITED

1. Jorgensen, B. B., and N. P. Revsbech. "Microsensors," *Methods in Enzymology*, **167**, 639 (1988).

2. Lewandowski, Z., P. Van Houdt, and B. Little. "Construction and Application of an Iridium Oxide pH Microelectrode," accepted for publication to *Biotechnology and Bioengineering*.

3. Weber, E. Electromagnetic Fields. John Wiley & Sons, Inc., New York (1950), 83-104, 145-7, 333-337.

4. Sadiku, M. Elements of Electromagnetics. Saunders College Publishing, Orlando, FL (1989), 184-189, 199-201, 257-263, 442-3.

5. Keithley Model 3322 LCR Meter, Owners Manual.

6. Smythe, W. R. Static and Dynamic Electricity. McGraw-Hill Book Company, Inc., New York (1950), 28-29, 33, 59-60.

7. Scott, A. H., and H. L. Curtis. "Edge Correction in the Determination of Dielectric Constant," *Journal of Research of the National Bureau of Standards*, **22**, 747 (1939).

8. Kirchhoff, G. "On the Theory of Condensers." *Monstsberichte Akademie der Wissenschaften zu Berlin*, 144 (1877)

9. Nicholson, J. W. "The Electrification of Two Parallel Circular Discs," *Philosophical Transactions of the Royal Society of London*, **224**, 303 (1924).

10. Savant, C. J., M. S. Roden, and G. L. Carpenter. Electronic Circuit Design. Benjamin/Cummings Publishing Company, Inc., Menlo Park, CA (1987), 376, A107-A113.

11. "Burr-Brown Integrated Circuits Data Book," **33**, Burr-Brown Inc., Tucson, AZ (1989), 2-21 - 2-26.

12. Hayt, W. H., and J. E. Kemmerly. Engineering Circuit Analysis. McGraw-Hill Book Company, Inc., New York (1986), 133, 378-379.

13. Characklis, W. G., and K. C. Marshall. Biofilms. John Wiley & Sons, Inc., New York (1990), 635-638.

14. Faires, J. D., and B. T. Faires. Calculus and Analytic Geometry. Prindle, Weber & Schmidt (PWS), Boston, MA (1983), 699-704.

15. Micro Kinetics Series CTC-283, Owners Manual.

16. Smyth, C. P., Dielectric Constant and Molecular Structure. Chemical Catalog Co., Inc., New York (1931).

17. Birks, J. B., and J. Hart. Progress In Dielectrics, Volume 3. John Wiley & Sons, Inc., New York (1961), 119.

18. Burfoot, J. C., and G. W. Taylor. Polar Dielectrics and Their Applications. University of California Press, Los Angeles, CA (1979).

19. Bard, A. J., and L. R. Faulkner. Electrochemical Methods (Fundamentals & Applications). John Wiley & Sons, Inc., New York (1980), 488-552.

20. Rieger, P. H. Electrochemistry. Prentice-Hall, Inc., Englewood Cliffs, NJ (1987), 108-124.

21. Martynov, G. A., and R. R. Salem. "Electrical Double Layer at a Metal-dilute Electrolyte Solution Interface," *Lecture Notes in Chemistry*, **33**, (1983).

22. Hanton, J. P. Design Using Electrical Engineering Materials. Department of Electrical Engineering, Montana State University, Bozeman, MT (September 1990).

23. Kassakian, J. G., M. F. Schlecht, and G. C. Verghese. Principles of Power Electronics. Addison-Wesley Publishing Co., Reading, MA (1991), 693-710.

24. Lutz, R. J., A. Menwat, and J.I. Peterson. "Polarographic Technique for the Determination of Effective Surface Area of Electrodes," *AIChe Journal*, **28**, 1027 (1982).

25. Lingane, P. J. "Chronopotentiometry and Chronoamperometry with Unshielded Planar Electrodes," *Analytical Chemistry*, **36**, 1723 (1964).

26. Dayton, M. A., J. C. Brown, K. J. Stutts, and R. M. Wightman. "Faradaic Electrochemistry at Microvoltammetric Electrodes," *Analytical Chemistry*, **52**, 946 (1980).

APPENDICES

APPENDIX A

MICRO KINETICS XYZ POSITIONING SYSTEM

Table 2 Micro Kinetics Positioning System

Quantity	Micro Kinetics Part Number	Description
1	CTC-462-2S	X-Y Positioning Table, 100 mm Travel
1	CTC-160-1	Z Positioning Arm, 25 mm Travel
1	CTC-283-3	3 Axis DC Motor Controller, RS-232 with LCD and Keypad for manual operation
2	CTC-322-20	22mm diameter encoder DC motors
2	CTC-321-21	24mm diameter gearheads 3088:1 ratio

APPENDIX B

SURFACE PROFILE OF A STAINLESS STEEL COUPON

Figure 19 Surface Profile of a Stainless Steel Coupon